arXiv:2206.09362v1 [cs.CV] 19 Jun 2022

Towards Generalizable Person Re-identification with a Bi-stream Generative Model

Xin Xu[a], Wei Liu[a], Zheng Wang[b], Ruimin Hu[b], Qi Tian[c]

[a]*School of Computer Science and Technology, Wuhan University of Science and Technology, Wuhan, China.*
[b]*School of Computer Science, Wuhan University, Wuhan, China.*
[c]*Huawei Noah's Ark Laboratory, Huawei Technologies Co Ltd, 115371 Shenzhen, Guangdong, China.*

Abstract

Generalizable person re-identification (re-ID) has attracted growing attention due to its powerful adaptation capability in the unseen data domain. However, existing solutions often neglect either crossing cameras (*e.g.,* illumination and resolution differences) or pedestrian misalignments (*e.g.,* viewpoint and pose discrepancies), which easily leads to poor generalization capability when adapted to the new domain. In this paper, we formulate these difficulties as: 1) Camera-Camera (*CC*) problem, which denotes the various human appearance changes caused by different cameras; 2) Camera-Person (*CP*) problem, which indicates the pedestrian misalignments caused by the same identity person under different camera viewpoints or changing pose. To solve the above issues, we propose a Bi-stream Generative Model (BGM) to learn the fine-grained representations fused with camera-invariant global feature and pedestrian-aligned local feature, which contains an encoding network and two stream decoding sub-network. Guided by original pedestrian images, one stream is employed to learn a camera-invariant global feature for the *CC* problem via filtering cross-camera interference factors. For the *CP* problem, another stream learns a pedestrian-aligned local

Xin Xu and Wei Liu are with the School of Computer Science and Technology, Wuhan University of Science and Technology, Wuhan 430081, China (e-mails: xuxin@wust.edu.cn, liuwei@wust.edu.cn). Zheng Wang and Ruimin Hu are with the School of Computer Science, Wuhan University, (email: wangzwhu@whu.edu.cn, hrm1964@163.com). Qi Tian is with the Huawei Noah's Ark Laboratory, Huawei Technologies Co Ltd, 115371 Shenzhen, Guangdong, China (email: tian.qi1@huawei.com).

feature for pedestrian alignment using information-complete densely semantically aligned part maps. Moreover, a part-weighted loss function is presented to reduce the influence of missing parts on pedestrian alignment. Extensive experiments demonstrate that our method outperforms the state-of-the-art methods on the large-scale generalizable re-ID benchmarks, involving domain generalization setting and cross-domain setting.

Keywords: Person Re-identification, Generalizable re-ID, Camera-Camera Problem, Camera-Person Problem

---

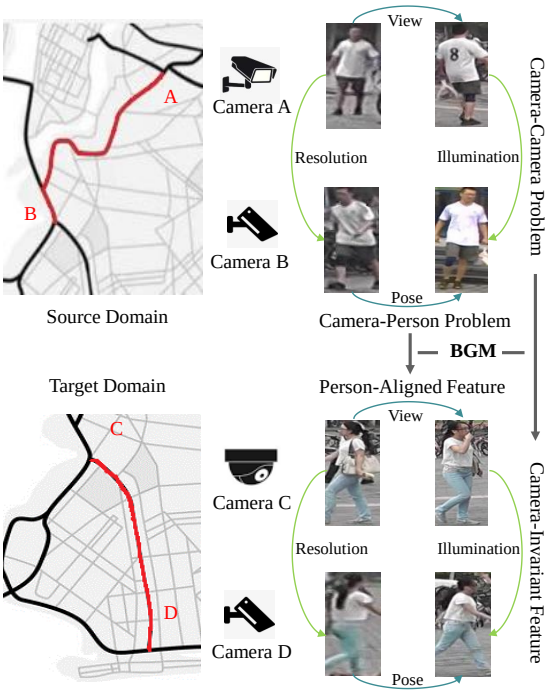

Figure 1: Generalizable re-ID usually suffers from the discrepancy of pedestrian appearance and pedestrian misalignment. The appearance discrepancy is caused by *CC* problem including difference of resolution, illumination, *etc.* which is shown by the green lines; while the change of viewpoint and pose, *etc.* in *CP* problem lead to misalignment as shown in the blue lines. The camera-invariant feature and pedestrian-aligned feature from the source domain can be learned by our BGM network, which can cope with the *CC* problem and *CP* problem in target domain, simultaneously.

1. Introduction

Person re-identification (re-ID) aims to retrieve pedestrian images across non-overlapping camera networks. In recent years, re-ID models trained and tested within a single data domain have achieved outstanding performance. However, when deployed to an unseen data domain, these re-ID models usually encounter a significant performance degradation due to the domain gap.

For practical deployment on an unseen domain, re-ID methods with generalization capability have received increasing attention. To achieve this goal, Unsupervised Domain Adaptation (UDA) [1, 2, 3, 4, 5, 6, 7, 8, 9, 10] methods are proposed to transfer the learned knowledge from the labeled source domain to an unlabeled target domain. Although the UDA methods are more practical than supervised re-ID methods, unlabeled data are still required to be collected from the target domain and used to update the model. To release these limitations, the Domain Generalization (DG) re-ID [11, 12, 13, 14, 15, 16, 17, 18] is proposed to train a cross-domain pedestrian retrieval model without any data from the target domain. The main idea of existing DG re-ID methods is to learn a domain-independent pedestrian feature. However, these methods ignore the impact of cameras (*e.g.,* illumination and resolution difference) or pedestrian image misalignment (*e.g.,* viewpoints and pose change), thus they still have a limited generalization capability when dealing with unseen data in the real world.

As shown in Figure 1, we formulated these challenges as: 1) Camera-Camera (CC) problem which puts barriers to the huge discrepancy in pedestrian appearance, caused by illumination differences, resolution differences, noise, and *etc.* across different cameras. 2) Camera-Person (CP) problem which leads to the misalignment of pedestrian images, caused by the change of pedestrian's viewpoint and pose to the camera. The appearance discrepancy and image misalignment pose huge challenges to re-ID. Furthermore, the unseen target domains bring unknown style variation and misalignment which leads to the domain gap between the source domain and target domain. The domain gap

raises difficulties for the generalizable re-ID task.

To address the above problems simultaneously, we propose a novel Bi-stream Generative Model (BGM) to learn the fine-grained representations fused by camera-invariant global feature and pedestrian-aligned local feature. The BGM consists of a feature encoding mainstream, a *CC* decoding stream, and a *CP* decoding stream. The two decoding streams share the same feature encoding network. The *CC* decoding stream learns the camera-invariant global feature by filtering out the randomly added interfering factors in the pedestrian image; while the pedestrian-aligned local feature is learned by *CP* decoding stream through aligning pedestrian images to a uniform UV space. Among them, the information-complete densely semantically aligned [19, 20, 21] part maps are designed to address the missing parts due to the *CP* problem, which are constructed through selecting the most information-complete 24 parts extracted from multiple images of the same identity pedestrian by DensePose [22]. To reduce the influence of missing parts on the pedestrian alignment, we design a part-weighted loss to guide the model paying more attention to easy-to-extract parts and less attention to hard-to-extract parts. The details of the method are described in Section III.

In summary, the main contribution of our work is threefold:

- We summarize the challenges in person re-ID into the Camera-Camera problem and the Camera-Person problem, and propose a novel Bi-stream Generative Model to solve both problems simultaneously.

- We are among the first attempt to use densely semantically aligned method to solve the generalization problem in the re-ID task. Moreover, we further propose to construct information-complete densely semantically aligned part maps to solve the problem of missing parts caused by the Camera-Person problem.

- To reduce the influence of missing parts on pedestrian alignment, a part-weighted loss based on the unbalanced number of parts is proposed to

guide the model paying more attention to the easy-to-extract parts and less to the hard-to-extract parts.

2. Related Works

2.1. Camera-Camera re-ID.

The *CC* problem caused by illumination difference, resolution difference, and noise, *etc.* leads to discrepancy in pedestrian appearance, which poses a challenge for re-ID, especially for generalizable re-ID [23, 24, 25, 26, 27, 28, 29]. Although there are many re-ID methods that have achieved good performance through representation learning, they usually assume that the pedestrian images have high resolution and the illumination does not change drastically. However, in real practice scenarios, illumination variations, resolution variations and even noise are present. Recently, some methods have been proposed for illumination variation [30, 31] and resolution variation [32, 33, 34, 35], respectively. However, all of these methods are only capable of solving one influencing factor alone, and lack a comprehensive consideration of various factors leading to CC problems.

In our BGM, the *CC* stream learns the camera-invariant global feature by filtering out randomly added interference factors in the pedestrian images, which can cope with various interference factors well.

2.2. Camera-Person re-ID.

The *CP* problem caused by the different viewpoints or poses of the pedestrian to the cameras leads to the misalignment of pedestrian images, which poses a great challenge for re-ID. In the early works, patch-based methods use fixed stripes or grids to segment the pedestrian images or feature maps to extract local features [36, 37, 38, 39, 40, 41, 42, 43, 44]. For example, Sun *et al.* [39] use attention mechanism to optimize the feature attention region and reduce the effect of misalignment on feature learning in fixed regions. To obtain more accurate attention regions to solve the problem of mismatched patches, human part/pose alignment is utilized to perform a similarity measurement among

the corresponding parts. For example, Ge *et al.* [45] used human key points to extract pose-irrelevant feature. However, although this method is highly accurate and can solve the misalignment problem well, it requires tedious human manual labeling of key points which is not practical in large-scale datasets. Then, Sun *et al.* [46] tried to use visible part awareness to determine which parts of the pedestrian are obscured and which parts are visible, and they do not need additional labels. Similarly, several methods adopted human pose estimation to locate human parts to reduce manual annotation [47, 48, 49, 50, 51, 52, 53, 54], thus aligning pedestrians at the part-level. However, these methods only use a few human key points, and encounter great challenges in cases of pedestrian occlusion.

The above methods have solved the pedestrian spatial misalignment problem at the coarse body part/pose level, but do not fundamentally solve the pedestrian misalignment caused by occlusion. Due to the different viewpoints of people to the cameras, the occlusion may occur with information loss. In [55], the densely semantically aligned (DSA) approach is proposed to generate densely texture by DensePose as alignment guidance to learn densely semantically aligned feature representation. However, the dense texture generated by DensePose is easily influenced by illumination variation and other interference factors caused by *CC* problem. Accordingly, we present a multi-frame compensation approach to solve the pedestrian image misalignment: 1) we make full use of the DensePose densely semantically aligned information and the visual information of multiple images of the same pedestrian to obtain a densely semantically part map with complete and aligned information; 2) we introduce a *CC* decoding stream to learn camera-invariant global feature which can assist the decoding task of information-complete densely semantically part map by reducing the impact of interference factors caused by *CC* problem such as illumination variation and noise.

2.3. Generalizable re-ID.

Despite the good performance within a single data domain, the fully supervised models usually show drastic performance degradation when being used in cross-domain pedestrian retrieval, due to the presence of the domain gap. Then the Unsupervised Domain Adaptation (UDA) methods were proposed to shrink the domain gap by using unlabeled data from target domain to update models. The UDA methods can be divided into style transfer [1, 2, 3], learning domain-invariant feature [4, 5, 6], and target domain pseudo-label estimation [7, 8, 9, 10]. Although UDA methods can reduce the domain gap to a certain extent, the target domain data required by them will bring difficulties in data collection and additional training consumption. Therefore, the Domain Generalization (DG) re-ID [11, 12, 13, 14, 15, 16] task that can be applied directly to unseen domains is raised. For reducing the influence of *CC* problem on domain gap, some DG methods normalize the style and content of the data from source domain by Instance Normalization (IN) and Batch Normalization (BN). Such like, The DualNorm [11] learns domain agnostic feature by jointly using IN and BN to normalize the style difference and content distribution. However, the instance normalization inevitably loses the discriminative information of the pedestrian while filtering the style variation. Then the Style Normalization and Restitution (SNR) [12] is also proposed to filter out the style shift by IN which is called Style Normalization (SN). Meanwhile, they introduced a restitution module, which reinstates discriminative information into the feature. Besides, the Camera-based Batch Normalization (CBN) [13] forces the data from different cameras to fall into the same subspace to decrease the distribution gap. However, above methods is trained on a single dataset which merely contains minor style variations and distribution gap. To this end, Song *et al.* [14] proposed a Domain-Invariant Mapping Network (DIMN) to associate images of pedestrians with their identity classifiers, so that multiple datasets for different training tasks share a single memory bank. Then Lin *et al.* designed a multi-dataset feature generalization network (MMFA-AAE) to learn domain-invariant features. However, all these methods only learn domain-invariant feature by reducing the influence of dis-

crepancy of pedestrian appearance due to *CC* problem, but ignore the effect of misalignment caused by CP *problem*. And unaligned pedestrian images have a significant influence on the feature matching process. Therefore, we propose a bi-stream generative model that can solve both the *CC* problem and the *CP* problem to improve the generalization capability.

3. Bi-stream Generative Model

We propose a novel Bi-stream Generative Model (BGM) to solve both the *CC* problem and the *CP* problem in re-ID. The proposed BGM consists of a mainstream feature encoding network and two decoding stream sub-networks. The *CC* decoding stream takes the original pedestrian image as the decoding target, and aims to guide the feature encoding network to learn a camera-invariant global feature by filtering various interference factors; while the *CP* decoding stream takes the information-complete densely semantically aligned part map as the decoding target, and aims to guide the feature encoding network to learn a pedestrian-aligned local feature by aligning the pedestrian image to a uniform UV space. Considering the two cases of poor image quality due to the *CC* problem and missing parts due to the *CP* problem, we propose an information-complete densely semantically aligned part map construction method based on the assumption that the pedestrian appearance does not change drastically in a short period of time. In addition, we discover that different parts have different extraction difficulties in the same dataset due to the fixed pedestrian viewpoint. In order to better utilize the important parts to guide the learning procedure of the model, we design a part-weighted loss function.

3.1. Main Stream Encoding Network

Our mainstream encoding network aims to learn a fine-grained representation fused by the camera-invariant global feature and the pedestrian-aligned local feature with the guidance of two decoding streams. The mainstream encoding network uses the sub-model of ResNet-50 [56], furthermore, to improve

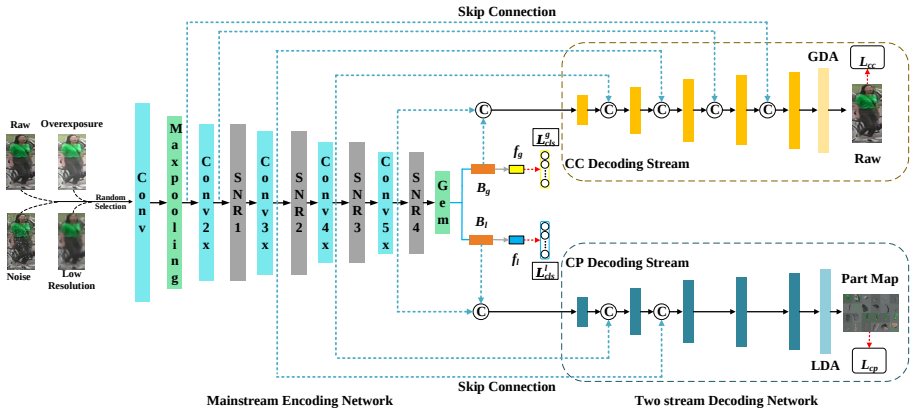

Figure 2: The structure of the bi-stream generative model. It contains a mainstream encoding network and two stream decoding sub-networks. The inputs of our encoding network are $P \times K$ images, and the fusion of global feature f_g and local feature f_l is learned by the encoding network with two classification loss functions as supervision. The CC stream takes the input images as ground truth with the CC Loss as supervision to mine the camera-invariant global feature, and the CP stream takes the information-complete densely semantic parts map as ground truth with CP Loss as supervision to let the pedestrian feature layer learn the pedestrian-aligned local feature. The B_g and B_l are two deconstructed identical bridging modules used to extend the halved 1024-channel features into 2048-channel to suit the input requirements of subsequent networks. The GDA/LDA represents global/local decoder adaptation which adapts the size of reconstruction results to the targets. Besides, the Gem is generalized mean pooling.

the generalization ability of the model, we use a plug-and-play SNR module to filter out the identity-irrelevant features. In addition, in order to make the camera-invariant global feature and the pedestrian-aligned local feature not conflict with each other during the learning procedure, we split the encoded 2048-channel feature map into two equal-sized 1024-channel features to learn the camera-invariant global feature and the pedestrian-aligned local feature respectively. In order to make the size of the features consistent with the input of the following decoding network, we introduce two structurally identical deconvolution bridge modules called B_g and B_l, respectively, to extend the two 1024-channel feature maps into 2048-channel, as shown in Figure 2. The fea-

tures F extracted by the mainstream encoding network and used in the final re-identification task can be computed as:

$$F = Gem\left((M(x))\right), \tag{1}$$

where x is the input pedestrian image, M is the mainstream encoding network, and Gem is the generalized mean pooling. The feature F is then split in half and fed into the two bridging modules Bg and Bl to obtain the camera-invariant global feature representation f_g and the pose independent pedestrian-aligned local feature representation f_l respectively. The $f_g = \mathbb{R}_g^{2048}$ and $f_l = \mathbb{R}_l^{2048}$ can be calculated as:

$$\begin{aligned} \mathbb{R}_{\mathrm{g}}^{2048} &= B_{\mathrm{g}}(C_g(F)), \\ \mathbb{R}_{\mathrm{l}}^{2048} &= B_{\mathrm{l}}(C_l(F)), \end{aligned} \tag{2}$$

where the $C_g(F)$ represents obtaining features in the $[1, 1024]$ dimension from the 2048 dimensional features and $C_l(F)$ represents obtaining features in the $[1025, 2048]$ dimension from the 2048 dimensional features. B_g and B_l are two deconstructed identical bridging modules used to expand f_g and f_l to 2048-channel respectively to suit the input requirements of subsequent decoding networks. Details of the bridging modules are shown in the Table 1.

3.2. Camera-Camera Decoding Stream.

Illumination differences, resolution differences, and noise of the *CC* problem lead to discrepancy in pedestrian appearance. In order to guide the mainstream feature encoding network to learn camera-invariant global feature, we take the form of encoding and decoding to filter out various interference factors which are randomly added to the pedestrian images. To avoid noise and other factors corrupting the original structure of pedestrian images and thus disturbing with feature encoding, our *CC* decoding stream adopts the skip connection structure in ResUNet to guarantee the decoding of the original pedestrian images. The skip connection can transfer the detailed information from the bottom layer to the top layer to assist the decoding task, and we input the features passed by

Table 1: The details of the network structure. Layer Name denotes the name of each module. Parameters denote the size of the convolution kernel. For example, $[3 \times 3, 1] \times 2$ means the size of the convolution kernel is 3, with stride value 1. And *trans* means the deconvolution ConvTranspose2d. If this subscript is absent, it means that the convolution operation is performed by stitching two modules with the same structure together in an orderly manner. GAP means the global average pooling.

Layer Name			Parameters	Output size
Bridge			$[3 \times 3, 1] \times 2$	$16 \times 4 \times 2048$
Global Decoder	UP Block	UP Sample	$[2 \times 2, 2]_{\text{trans}} \times 1$	-
		Conv Block1	$[3 \times 3, 1] \times 2$	-
		Conv Block2	$[3 \times 3, 1] \times 2$	-
	GDA		$[1 \times 1, 1] \times 1$	$256 \times 128 \times 3$
Local Decoder	LDA		$[1 \times 1, 1] \times 1$ GAP	$128 \times 192 \times 3$

the skip connection into the upsampling module for decoding after the concatenate operation with the corresponding features of the decoding sub-network, as shown in Figure 2. In order to make the output compatible with the size of input pedestrian image, we add the size adaptation module which we call Global Decoder Adaptation module (GDA) before the final image reconstruction. To fully utilize all the encoding features, we transfer features output from each layer of the mainstream feature encoding network to the corresponding layer of the *CC* decoding stream through the skip connection. We define the features of the mainstream encoding network as $df = \{df_i \mid i \in 0, 1, \ldots, 4\}$, and the output of the feature upsampling module in the *CC* decoding stream as $uf^g = \{uf_i^g \mid i \in 5, 4, \ldots, 1\}$.

The reconstruction of original pedestrian image can be calculated as:

$$\begin{aligned} uf_{i+1}^g &= \left(GUP_i\left(CAT_i^g\left[uf_i^g, df_i\right]\right)\right), \\ \widehat{\mathrm{G}}^x &= GDA(uf_{final}^g) \end{aligned} \tag{3}$$

where CAT_i^g concatenates the $i-th$ encoding layer feature map with the corresponding $i-th$ global decoding layer feature map by channel. GUP_i indicates

the $i-th$ global upsampling block. uf^{g}_{final} denotes the output of the last CC stream upsampling block. The details of the modules mentioned above are shown in the Table 1.

3.3. Camera-Person Decoding Stream.

The change of viewpoint and pose of the pedestrian to the camera in the CP problem leads to the misalignment of the pedestrian images, which will pose a challenge to the matching of pedestrian features. To solve this problem, we adopt DensePose to extract the human parts in the pedestrian images and then align these parts to a uniform UV coordinate space. However, when low-quality pedestrian images are input or when there are occlusions in the images, *etc.*, the missing parts phenomenon occurs because DensePose fails to extract the traveler parts. To solve this problem, we propose an information complete construction method for densely semantically aligned part map. In addition, to better guide the mainstream feature encoding network to learn pedestrian-aligned local feature, we design a CP decoding stream that is asymmetric to the CC decoding stream.

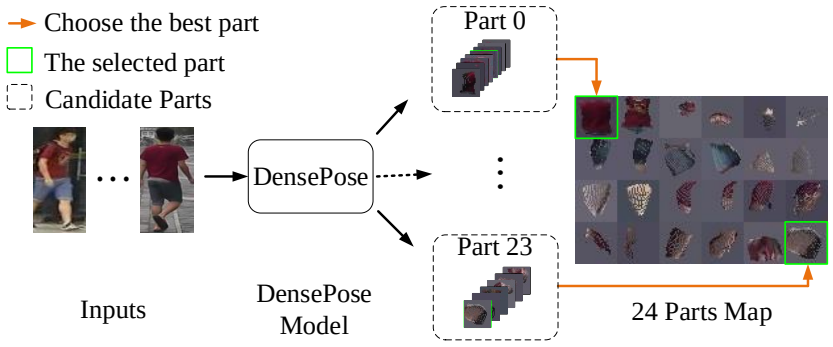

Figure 3: Pedestrian images with the same label from the training data are fed into the DensePose model to classify the output parts into 24 categories. The 24 parts map is populated with the part containing the information-complete densely semantics, respectively.

3.3.1. Information-complete densely semantically aligned parts map construction.

Similar to the DSA [55], we also construct our densely semantically aligned part map with the help of DensePose. Furthermore, for the case of missing parts due to *CP* problem, we propose an information-complete densely semantically aligned part map construction method, and the flow of the method is shown in Figure 3. Furthermore, in this section, we discuss the advantages and possible limitations of the method.

1) Information-complete densely semantically part search and parts map construction. The visual features used to distinguish the identity of the same pedestrian are essentially the same for a limited period of time. In other words, different images of the same identity pedestrian in a pixel-level densely semantically aligned spatial map can extract parts with the same semantics. However, the amount of information contained in these parts extracted from different images of that pedestrian is different, even though these parts have the same semantics. It is observed that the pixel-level semantic information is not accurate, when DensePose is deployed on some re-ID datasets containing low-quality images. To this end, we statistic the content information for each part, and naturally assume that the part with more pixel points contains more semantic information. The information-complete densely semantically part search method can be formulated as:

$$\begin{aligned} Part_i^x &= \{DP(x_j) \mid j \in index^x, i \in 0, \ldots, 23\} \\ Parts^x &= \{\max(pixs(Part_i^x)) \mid i \in 0, \ldots, 23\}, \end{aligned} \tag{4}$$

where $DP(x_j)$ denotes the $j-th$ image of the pedestrian x, and is used as input of the DensePose model to generate 24 parts. The background of each part is filled with the average of the pixels of the whole image input with a size of 32×32. $index^x$ denotes the image number of the pedestrian x, $pixs$ denotes the number of foreground pixel points in the statistical part. As shown in Figure 3, all the selected 24 densely semantically aligned parts are filled into the 128×192 size image space, thus obtaining a densely semantically aligned

parts map with complete information.

2)Discussion: The information-complete densely semantically aligned parts map has the following three main advantages. (*i*) The information-complete densely semantically aligned part map aligns pedestrian images into a uniform UV space, thus reducing the impact of pedestrian image misalignment on re-ID due to *CP* problem. (*ii*) This part map consists of parts extracted from multiple images of the same pedestrian, which can effectively solve the problem of missing parts and poor part quality due to occlusion or other factors. (*iii*) Since only the features encoded by the mainstream encoding network are needed during testing procedure and the part maps are not required, it is not necessary to generate the densely semantically aligned part maps corresponding to the test set. Further, the part map is automatically extracted by DensePose without manual labeling, which can save manpower largely.

However, such images for pedestrian re-ID task also have some drawbacks, mainly three: (*i*) Since DensePose is prone to fail in some low-quality images of pedestrian re-ID datasets, which cannot totally be solved by multiple images completion. (*ii*) The dramatic changes in visual features occur on the multiple images of the same pedestrian, caused by varying environment illumination, resolution or other factors in a short time. Then, the image reconstruction on multiple inputs is unable to guarantee a satisfied output. (*iii*) Although we use a multiple-image complementation approach to construct as complete a part map as possible, however, there are still many pedestrians, in some public re-ID datasets, that cannot generate a complete part map.

3.3.2. Network Details

Since the pose changes and viewpoint changes of the pedestrian to camera in the *CP* problem lead to pedestrian image misalignment, we design a *CP* decoding stream to guide the mainstream feature encoding network to learn the pedestrian-aligned local feature. This decoding sub-network also adopts the skip connection structure of ResUNet for transferring features from the encoding layers to the decoding network. Different from the *CC* stream, we only

transfer the top three semantic features to the decoding stream through the skip connection and concatenate them with the corresponding features to be input to the following upsampling modules. Besides, in order to make the output compatible with the size of input information-complete densely semantically part map, the Local Decoder Adaptation module (LDA) is introduced before the final image reconstruction. The *CP* stream also adopts the five upsampling modules with the same structure as the *CC* stream, and the output features of each upsampling module are defined as $uf^l = \left\{uf_i^l \mid i \in 5, 4, \ldots, 1\right\}$. The information-complete densely semantically parts map reconstruction result $\widehat{\mathrm{P}}^x$ can be calculated as:

$$\begin{aligned} uf_{i+1}^l &= \left(LUP_i\left(CAT_i^l\left[uf_i^l, df_i^{'}\right]\right)\right), \\ \widehat{\mathrm{P}}^x &= LDA(uf_{final}^l) \end{aligned} \tag{5}$$

where CAT_i^l concatenates the $i-th$ encoding layer feature map with the corresponding $i-th$ local decoding layer feature map by channel. LUP_i indicates the $i-th$ local upsampling block. uf_{final}^l denotes the output of the last *CP* stream upsampling block. $df^{'} = \{df_i \mid i \in 2, 3, 4\}$, which contains only the last three layers of all skip connections, and is used to facilitate the local reconstruction task.

3.4. Loss function

For each task in our three streams, we design appropriate loss function to optimize it.

For the feature learning task in the mainstream feature encoding network, ID Loss and Triplet Loss are jointly utilized for pedestrian identity classification to learn robust representations. The classification loss L_{cls} can be calculate as:

$$\begin{aligned} \mathcal{L}_{\mathrm{cls}} &= \mathcal{L}_{id} + \mathcal{L}_{tri} \\ \mathcal{L}_{id} &= \tfrac{1}{N}\textstyle\sum_{i=1}^{N}\left(-y_i \cdot \log p\left(x_i\right)\right) \\ \mathcal{L}_{tri} &= \tfrac{1}{N}\textstyle\sum_{i=1}^{N}\left(d_{\max}\left(x_i, x_i^p\right) - d_{\min}\left(x_i, x_i^n\right) + m\right), \end{aligned} \tag{6}$$

where N is the batch size, x_i and y_i denote the $i-th$ image and its identity label. $p(x_i)$ means the predicted identity of x_i. $d_{\max}$ represents maximum the distance of positive pairs x_i and x_i^p. Accordingly, $d_{\min}$ represents minimum the distance of negative pairs x_i and x_i^n. m is margin.

For the original pedestrian image reconstruction task in the CC stream, CC Loss L_{cc} is used to minimize the L1 distance between the reconstruction results and the target images. For the CC stream, the original input image is used as the supervised signal. The CC Loss L_{cc} can be calculate as:

$$L_{cc} = \frac{\sum_{i=1}^{N} \left| \widehat{\mathrm{G}_i}^{x} - x_i \right|}{\mathrm{N}}, \tag{7}$$

where $\widehat{\mathrm{G}_i}^{x}$ denotes the global image generation result of $i-th$ image of pedestrian x. While for the CP stream, we use the information-complete densely semantically aligned parts map as the supervised signal. For pedestrians with the same ID, this local stream uses the same densely semantically aligned parts map.

As for the reconstruction task of the information-complete densely semantically aligned part map in the CP decoding stream, the information-complete densely semantically aligned part map is used as the supervisory signal. While constructing the information-complete densely semantically aligned part maps, we counted the number of different parts in each dataset as shown in the Table 2. We found that there are large differences in the number of occurrences of parts with different semantics. For better exploitation of the easily extracted important parts to guide the mainstream feature coding network to learn pedestrian-aligned local feature, we design a loss function L_{cp} that weights the parts with different semantics according to the number of parts thereby minimizing the L1 distance between the decoded part map from the CP stream and its corresponding densely semantically aligned part map. The L_{cp} can be calculated as:

$$L_{cp} = \frac{\sum_{i=1}^{N} \sum_{j=1}^{24} \left| \widehat{\mathrm{P}_i^j} - \mathrm{Parts_j} \right| * \frac{\mathrm{PartNum}_j}{\mathrm{PartSum}}}{\mathrm{N}} \tag{8}$$

Table 2: Statistical results for the number of 24 semantic parts in the CUHK02, CUHK03, CUHK-SYSU, Market-1501, DukeMTMC-reID datasets. The part with the number from "0" to "23" represent "back", "front chest", "left hand", "right hand", "left foot", "right foot", "back left thigh", "back right thigh", "front left thigh", "front right thigh", "back left calf", "back right calf", "front left calf", "front right calf", "back left thigh", "back right thigh", "front left thigh", "front right thigh", "back left thigh", "back right thigh", "front left thigh", "front right thigh", "front left thigh", "front right thigh", "back left thigh", "front right thigh", "back left thigh", "back right thigh", "front left thigh", "front right thigh", "front left thigh", "front left thigh", "front right thigh", "left head", "right head".

Part	CUHK02	CUHK03	CUHK-SYSU	Market-1501	DukeMTMC-reID	Total
0	4834	10031	21688	16498	23897	76948
1	6297	12985	30473	25211	33223	108189
2	3428	6601	17478	13198	13043	53748
3	3684	6919	17633	12904	12079	53219
4	5499	8871	18601	8987	20987	62945
5	5333	8913	18414	8589	21220	62469
6	3371	6275	14143	6619	13076	43484
7	3175	6161	13755	5887	12384	41362
8	6134	12399	26511	16647	29333	91024
9	5858	11724	26422	15955	27974	87933
10	3077	5676	11933	4319	12441	37446
11	2874	5035	11795	3906	11179	34789
12	6294	11810	24061	13379	27660	83204
13	6369	11685	24411	13825	27541	83831
14	4101	8037	20043	14805	20426	67412
15	3934	8166	19915	13910	20834	66759
16	5620	10215	24500	17745	22683	80763
17	5610	10129	24217	17199	23297	80452
18	3456	5065	14000	9627	9346	41494
19	3080	4926	12627	7345	8254	36232
20	4856	8623	21771	14616	19512	69378
21	4858	8761	21145	14317	20315	69396
22	6209	11967	30037	24309	29080	111602
23	5918	11184	29648	23932	28334	99016
PartSum	113869	212158	495221	323729	488118	1633095

where $\widehat{\mathrm{P}_i^j}$ and $Parts_j$ denote the densely semantic parts map generation result of $j-th$ part in $i-th$ image of pedestrian x and the $j-th$ part of $Parts^x$, respectively. $\mathrm{PartNum}_i$ and PartSum represent the number of $j-th$ part and the total number of all parts in the source domain, respectively.

To make both the camera-invariant global feature and the pedestrian-aligned local feature to be more discriminative, classification loss L_{cls} is added for their constraints separately. To compute the identity verification loss, the classifiers are added to both global feature and local feature to output the probability of classification. Finally, the loss function of the bi-stream generative model L_{BGM} can be calculated as :

$$L_{BGM} = L_{cls}^g + L_{cls}^l + L_{cc} + L_{cp}, \tag{9}$$

where L_{cls}^g and L_{cls}^l denote the classification loss of the camera-invariant global feature and the pedestrian-aligned local feature, respectively.

4. Experiments

4.1. Datasets and Evaluation Metrics

Datasets. To evaluate the effectiveness of our method, in addition to the conventional train/test on a single dataset, we adopt the same experimental setup as DIMN [14] and DualNorm [11]. In this experimental setup, multiple large-scale datasets are jointly used to train the model. Several small-scale but challenging datasets are used to test the generalization performance of the model. In our experiments, CUHK02 [57], CUHK03 [42, 58], CUHK-SYSU [59], Market-1501 [60], and DukeMTMC-reID [61] are used as training sets. To take advantage of more data from different domains, we use all the images in the large datasets to train our model, ignoring the existing train/test splits in these datasets. All five large-scale datasets with 121,765 images from 18530 IDs and information-complete densely semantically aligned part maps corresponding to the IDs were used to train our model. Four additional small-scale but challenging

Table 3: Dataset details.

Datasets	IDs	Images	Cameras
CUHK02	1816	7264	10
CUHK03	1467	13164	10
CUHK-SYSU	11934	34574	-
Market-1501	1501	32217	6
DukeMTMC-reID	1812	36411	8
VIPeR	632	1264	2
PRID	934	24541	2
GRID	1025	1275	8
i-LIDS	119	476	2

datasets VIPeR [62], PRID [63], GRID [64], and i-LIDS [65] were used to test our model. The details of these above datasets are shown in Table 3.

Evaluation Metrics. We adopt cumulative matching characteristics (CMC) at rank-k and mean average precision (mAP) as evaluation metrics.

4.2. Implementation Details

Network settings. We utilize part of ResNet-50 [56] structure ($conv1$, $conv2_x$, $conv3_x$,$conv4_x$ and $conv5_x$) to build our baseline network and initialize it with the ImageNet [66] pretrained model. Considering the help of SNR [12] module for the model to learn generalizable re-id feature representation, we add the plug-and-play SNR module after each convolution. The two stream decoding sub-networks are initialized by the widely used Kaiming initialization [67] to obtain a faster convergence rate. For the *CC* decoding sub-network, we use $\mathrm{cat}\,(uf_5^g, df_4)$, $\mathrm{cat}\,(uf_4^g, df_3)$, $\mathrm{cat}\,(uf_3^g, df_2)$, $\mathrm{cat}\,(uf_2^g, df_1)$, and $\mathrm{cat}\,(uf_1^g, df_0)$ as inputs to the five upsampling blocks; while for the *CP* decoding sub-network, we use $\mathrm{cat}\left(uf_5^l, df_4\right)$, $\mathrm{cat}\left(uf_4^l, df_3\right)$, $\mathrm{cat}\left(uf_3^l, df_2\right)$, uf_2^l, and uf_1^l as inputs to the five upsampling blocks, where *cat* indicates that the feature maps are concatenated by channel. Note that the upsampling blocks of the two sub-networks do not share weights.

Data augmentation. In our approach, we use the commonly used random cropping [68], horizontal flipping, and random erasing [68, 69, 70] (probability parameter set to 0.5) data enhancement methods to help the network learn a robust feature representation of pedestrian.

Optimization. We obtain a mini-batch of our images by triplet loss with batch hard mining, where pedestrian classes P is set to 16, and the number of images in each class K is set to 4. The L_{cls}^{g}, L_{cls}^{l}, L_{cc}, and L_{cp} are set to equal weights. We use SGD optimizer and set the weight decay to 5×10^{-4} to train the model. For the first 10 epochs, we used a linearly increasing learning rate from 3×10^{-4} to 3×10^{-2}. After then, the learning rate decreases by a weight decay factor of 0.1 at 60, 100, and 150 epochs, respectively. The network reaches convergence in 200 training epochs.

Table 4: Performance (%) comparison with State-of-the-Art on domain generalization setting. "R1", "R5", "R10" denote "Rank-1", "Rank-5", "Rank-10" respectively. The best/sub-optimal results are marked with boldface/underline.

Methods	VIPeR				PRID				GRID				i-LIDS			
	R1	R5	R10	mAP	R1	R5	R10	mAP	R1	R5	R10	mAP	R1	R5	R10	mAP
Switchable (BN+IN) [71]	51.6	72.9	80.8	61.4	59.6	<u>78.6</u>	<u>90.1</u>	<u>69.4</u>	39.3	<u>58.8</u>	<u>68.1</u>	<u>48.1</u>	<u>77.3</u>	**91.2**	<u>94.8</u>	**83.5**
MMFA-AAE [15]	**58.4**	-	-	-	57.2	-	-	-	<u>47.4</u>	-	-	-	**84.8**	-	-	-
DIMN [14]	51.2	70.2	76.0	60.1	39.2	67.0	76.7	52.0	29.3	53.3	65.8	41.1	70.2	89.7	94.5	78.4
DualNorm [11]	53.9	-	-	-	<u>60.4</u>	-	-	-	41.4	-	-	-	74.8	-	-	-
BGM (ours)	<u>56.5</u>	**77.3**	**81.8**	**65.2**	**69.0**	**87.0**	**91.0**	**76.3**	**47.8**	**64.2**	**71.9**	**55.1**	75.0	<u>90.0</u>	**95.0**	<u>81.5</u>

4.3. Comparison with State-of-the-Arts

4.3.1. Domain Generalization.

We compared the proposed BGM network with the aforementioned methods for DG re-ID. The source/target domain splits methods [15, 72, 14] are adopted. The training source domain datasets contain CUHK02, CUHK03, Market-1501, DukeMTMC-reID and CUHK-SYSU PersonSearch. The testing target domain datasets contain VIPeR, PRID, GRID and i-LIDS. The results are shown in Table 4.

VIPeR. The performance of BGM is 1.9% lower on the rank-1 metric than the MMFA-AAE [15] method due to the fact that they use additional labels for

the domains. The BGM achieves the best performance on the rank-5, rank-10 and mAP metrics and outperforming the sub-optimal method by +4.4%, +1.0% and +3.8% respectively.

PRID. The BGM achieves the best performance in rank-1, rank-5, rank-10, and mAP metrics, outperforming the sub-optimal by +8.6%, +8.4%, +0.9%, and +6.9% respectively.

GRID. The BGM achieves the best performance in rank-1, rank-5, rank-10, and mAP metrics, outperforming the sub-optimal by +0.1%, +5.4%, +3.8%, and +7.0% respectively.

i-LIDS. The BGM achieves the best result on the rank-10 metric, +0.2% higher than the sub-optimal. And the BGM achieves the sub-optimal result on the rank-5 and mAP metrics, 1.2% and 2.0% lower than the best method, respectively.

The results of the above experiments illustrate that our BGM method has good generalization capability due to the good solution to the *CC* problem and the *CP* problem.

Table 5: Performance (%) comparison with State-of-the-Art on the cross-domain setting. "R1", "M" and "D" denotes "Rank-1", "Market-1501", and "DukeMTMC-reID", respectively. The best/sub-optimal results are marked with boldface/underline.

Methods	Source	Target: D		Source	Target: M	
		R1	mAP		R1	mAP
IBN-Net [73]	M	43.7	24.3	D	50.7	23.5
OSNet [74]	M	44.7	25.9	D	52.2	24.0
OSNet-IBN [74]	M	47.9	27.6	D	57.8	27.4
OSNet-AIN [74]	M	52.4	30.5	D	61.0	30.6
MuDeep [72]	M	47.6	27.7	D	-	-
SNR [12]	M	55.1	<u>33.6</u>	D	<u>66.7</u>	33.9
QAConv [16]	M	48.8	28.7	D	58.6	27.2
MetaBIN [17]	M	<u>55.2</u>	33.1	D	**69.2**	**35.9**
BGM (ours)	M	**55.6**	**35.9**	D	65.7	<u>35.8</u>

4.3.2. Cross-Domain.

In addition, to further validate the generalization ability of the BGM, we conducted a cross-domain experimental setting. And the BGM is compared with the state-of-the-art methods including omni-scale network (OSNet) [74] and the multi-scale deep learning model (MuDeep) [72], which utilize multi-scale information, the IBN-Net [73], the SNR [12], and the MetaBIN[17], which utilize a combination of IN and BN, and the QAConv [16], which utilizes local matching. As it is shown in Table 5, when the model is trained in the Market-1501 and tested on the DukeMTMC-reID, BGM achieves 55.6% rank-1 accuracy and 35.9% mAP accuracy which is better than the sub-optimal MetaBIN [17] by +0.4% and SNR [12] +2.3%, respectively. The BGM also achieves competitive results when the model is trained on DukeMTMC-reID and tested on Market-1501. Although the performance is slightly lower than the Meta-BIN method, this is mainly due to the fact that the Meta-BIN method utilizes a more complex meta-learning approach to train model, which will significantly increase the training complexity and convergence time of the model.

4.3.3. Supervised re-ID.

Since the *CC* problem and *CP* problem affect the supervised re-ID task, we compared the BGM with the state-of-the-art methods to solve the *CP* problem on the Market-1501 and DukeMTMC-reID datasets to validate the performance of the BGM, and the results are shown in Table 6. On the Market-1501, BGM (Re-Rank) achieves the best result on the mAP metric and is +3.9% above the sub-optimal; and achieves the sub-optimal results on the rank-1 metric, i.e. 0.2% lower than the SAN [80]. However, the SAN is based on generated images. Besides, BGM (Re-Rank) achieves better results than the SAN on the mAP metric, and on both the rank-1 and mAP metrics on the DukeMTMC-reID dataset. Although the performance is slightly lower than the HRS method, this is mainly due to the introducing of a weakly-supervised region segmentation method to predict informative regions, which will significantly increase the training complexity and convergence time of the model.

Table 6: Performence (%) comparisons with the State-of-the-Art methods on the Market-1501 and DukeMTMC-reID datasets. The best/sub-optimal results are marked with boldface/underline. "R1" denotes "Rank-1".

Method		Market-1501		DukeMTMC	
		R1	mAP	R1	mAP
Patch-based	PCB+RPP [39]	93.8	81.6	83.3	69.2
	VPM [46]	93.0	80.8	83.6	72.6
	HPM [75]	94.2	82.7	86.6	74.3
	MGN [40]	95.7	86.9	88.7	78.4
	HRS [76]	95.5	<u>89.4</u>	**90.8**	**80.8**
Part/Pose-related	Spindle [49]	76.9	-	-	-
	IDE [39]	85.3	68.5	73.2	52.8
	SPReID [77]	92.5	81.3	84.4	71.0
	FD-GAN [45]	90.5	77.7	80.0	64.5
	Part-Aligned [53]	91.7	79.6	84.4	69.3
	Pose Transfer [78]	87.7	68.9	68.6	48.1
	FEPB [79]	92.7	81.3	86.2	72.6
Pixel-level alignment	DSA [55]	95.7	87.6	86.2	74.3
	SAN [80]	**96.1**	88.0	87.9	75.5
Ours	BGM	95.6	87.8	89.0	77.3
	BGM(Re-Rank)	<u>95.9</u>	**93.3**	<u>89.7</u>	<u>78.5</u>

Table 7: Ablation Results. "R1", "M", "D" denote "Rank-1", "Market-1501", "DukeMTMC-reID", respectively. The best/sub-optimal results are marked with boldface/underline.

Methods	Source	Target: D		Source	Target: M	
		R1	mAP		R1	mAP
Baseline	M	46.3	30.0	D	60.8	31.6
BGM-CC	M	47.9	30.5	D	62.7	33.0
BGM-CP *w/o* L_{cp}	M	49.6	31.5	D	64.5	33.4
BGM *w/o* L_{cp}	M	<u>55.3</u>	<u>35.8</u>	D	<u>65.1</u>	<u>34.8</u>
BGM *w/o cutting*	M	49.0	31.7	D	60.8	30.5
BGM	M	**55.6**	**35.9**	D	**65.7**	**35.8**

4.4. Ablation Study

Behavioral analysis of the *CC* stream. We explore the effect of the *CC* decoding stream on person re-ID feature representation in this section. Here we only consider the reconstruction of input pedestrian images. We use the prefix "BGM" to denote the bi-stream generative model under different modules and settings, as shown in Table 7, the "BGM-CC" denotes the addition of the *CC* stream decoding sub-network to the main stream encoding network. It can be seen that our "BGM-CC" has a $+1.6\%/+0.5\%$ improvement in rank-1/mAP accuracy compared with the baseline when the source domain dataset is Market-1501 and the target domain dataset is DukeMTMC-reID. Moreover, when the source domain dataset is DukeMTMC-reID and the target domain dataset is Market-1501, "BGM-CC" also has a $+1.9\%/+1.4\%$ improvement in rank-1/mAP accuracy compared to the baseline. In addition to objective performance improvements, as can be seen in Figure 4, the *CC* decoding stream can effectively mine pedestrian identity information, and some interfering factors, such as pedestrians in the background (indicated by red boxes), cannot be detected in the generation sub-task and appear ambiguous (indicated by green boxes).

The availability of information-complete densely semantically aligned

Figure 4: The first row shows the input images and the second row shows the image reconstruction results of our "*CC* stream". It can be seen that the background pedestrian (shown in red), which is a disadvantage for the person re-ID task, almost disappears in the output of the *CC* stream decoding network (shown in green).

parts information. Although the *CC* stream decoding sub-network module can improve the performance well, the pedestrian misalignment caused by *CP* problem has not been solved yet. To this end, we introduce a *CP* decoding stream sub-network (labeled as "BGM-CP *w/o* L_{cp}") to learn the pedestrian-aligned local feature, which will learn the densely semantically aligned feature from the misaligned pedestrian image with the help of information-complete densely semantically aligned part map. Here, we consider the effect of the part map itself under the constraint of a simple L1loss. Compared with the baseline, the performance of *CP* decoding stream sub-network is further improved by $+3.3\%/+1.5\%$ in rank-1/mAP accuracy when the source domain dataset is Market-1501 and the target domain dataset is DukeMTMC-reID. Moreover, when the source domain dataset is DukeMTMC-reID and the target domain dataset is Market-1501, "BGM-CP *w/o* L_{cp}" also has a $+3.7\%/+1.8\%$ improvement in rank-1/mAP accuracy compared to the baseline. Based on the decoding results of the *CP* stream shown in Fig 5, we can conclude that the decoding target of a densely semantically aligned parts map with complete information leads the model to rebuild the missing parts (indicated by green boxes) due to viewpoint or pose, *etc.* This pedestrian-aligned local feature learned by *CP* stream results in a large performance improvement of the model.

Holistic analysis of bi-stream generative model. As a bi-stream gen-

Figure 5: The first column shows the pedestrian images with different IDs, and the next three columns are the results generated by *CP* stream with the top 24, top 12, and top 4 number of parts constituting the part map as the local generation sub-network generation target, respectively. The body parts in the green box indicate the missing parts in the pedestrian image due to changes of pose or viewpoint.

erative model that solves both *CC* and *CP* problems, the two decoding streams complement each other more than they perform on their own. As shown in the table 7, the complete bi-stream generative model (BGM) outperforms baseline in the experimental setting from Market-1501 to DukeMTMC-reID by $+9.0\%/+5.8\%$ in rank-1/mAP accuracy. Meanwhile, the "BGM *w/o* L_{cp}" achieves a performance improvement over baseline in the experimental setting from DukeMTMC-reID to Market-1501 $+4.3\%/+3.2\%$. More surprisingly, the improvement of the "BGM *w/o* L_{cp}" network over the baseline model is even greater than the sum of the improvements of the *CC* stream and the *CP* stream for baseline, respectively, which can indicate the complementarity between the Camera-Camera decoding and Camera-Person decoding tasks. In addition, considering the unbalanced number of parts due to missing parts, we design a loss

function L_{cp} with the number of different parts for weighting to constrain the CP decoding task. In the table, it can be seen that the performance of "BGM" with the addition of the proposed L_{cp} has another $+0.3\%/+0.1\%$ improvement in rank-1 and mAP accuracy, respectively, when the model trained on Market-1501 is tested on DukeMTMC-reID; while BGM achieves $+0.6\%/+1.0\%$ improvement in rank-1 and mAP accuracy, respectively, when the model trained on DukeMTMC-reID is tested on Market-1501. Additionally, "BGM *w/o cutting*" represents directly feeding the encoding network feature into the decoding network without cutting it in half. It can be found that the performance drops by 6.6%/4.2% for rank-1/mAP on DukeMTMC-reID and by 4.9%/5.3% for rank-1/mAP on Market-1501 respectively, demonstrating the effectiveness of our feature halving.

5. Conclusion

In this paper, we summarize the challenges in person re-identification and decouple them as two types of problems, *e.g.*, the Camera-Camera (CC) and the Camera-Person (CP). The domain gap caused by these problems poses a challenge to generalizable re-ID. To address this challenge, we propose a novel Bi-stream Generative Model (BGM) to solve the CC and CP problems simultaneously. With the two stream decoding sub-networks, the main stream learns camera-invariant global feature to cope with the appearance discrepancy and pedestrian-aligned local feature to solve the misalignment of pedestrian images. Besides, we propose a loss function based on the imbalanced number of parts to guide the model paying more attention to easy-to-extract parts and less on hard-to-extract parts. Extensive experiments verified that our model shows outstanding generalization capacity without any prior information from the target domain. In conclusion, we define two categories of problems that have a significant impact on person re-identification, especially generalizable re-identification, and propose a bi-stream generative model and a part-weighted loss function to solve them at the same time.

References

[1] W. Deng, L. Zheng, Q. Ye, G. Kang, Y. Yang, J. Jiao, Image-image domain adaptation with preserved self-similarity and domain-dissimilarity for person re-identification, in: CVPR, 2018, pp. 994–1003.

[2] J. Liu, Z.-J. Zha, D. Chen, R. Hong, M. Wang, Adaptive transfer network for cross-domain person re-identification, in: CVPR, 2019, pp. 7202–7211.

[3] L. Wei, S. Zhang, W. Gao, Q. Tian, Person transfer gan to bridge domain gap for person re-identification, in: CVPR, 2018, pp. 79–88.

[4] Z. Zhong, L. Zheng, Z. Luo, S. Li, Y. Yang, Invariance matters: Exemplar memory for domain adaptive person re-identification, in: CVPR, 2019, pp. 598–607.

[5] J. Li, S. Zhang, Joint visual and temporal consistency for unsupervised domain adaptive person re-identification, in: ECCV, 2020, pp. 483–499.

[6] D. Mekhazni, A. Bhuiyan, G. Ekladious, E. Granger, Unsupervised domain adaptation in the dissimilarity space for person re-identification, in: ECCV, 2020, pp. 159–174.

[7] X. Zhang, J. Cao, C. Shen, M. You, Self-training with progressive augmentation for unsupervised cross-domain person re-identification, in: ICCV, 2019, pp. 8222–8231.

[8] Y. Fu, Y. Wei, G. Wang, Y. Zhou, H. Shi, T. S. Huang, Self-similarity grouping: A simple unsupervised cross domain adaptation approach for person re-identification, in: ICCV, 2019, pp. 6112–6121.

[9] J. Chen, J. Qin, Y. Yan, L. Huang, L. Liu, F. Zhu, L. Shao, Deep local binary coding for person re-identification by delving into the details, in: ACM MM, 2020, p. 3034–3043.

[10] Y. Zhai, S. Lu, Q. Ye, X. Shan, J. Chen, R. Ji, Y. Tian, Ad-cluster: Augmented discriminative clustering for domain adaptive person re-identification, in: CVPR, 2020, pp. 9021–9030.

[11] J. Jia, Q. Ruan, T. M. Hospedales, Frustratingly easy person re-identification: Generalizing person re-id in practice, in: BMVC, 2019, pp. 141.1–141.14.

[12] X. Jin, C. Lan, W. Zeng, Z. Chen, L. Zhang, Style normalization and restitution for generalizable person re-identification, in: CVPR, 2020, pp. 3143–3152.

[13] Z. Zhuang, L. Wei, L. Xie, T. Zhang, H. Zhang, H. Wu, H. Ai, Q. Tian, Rethinking the distribution gap of person re-identification with camera-based batch normalization, in: ECCV, 2020, pp. 140–157.

[14] J. Song, Y. Yang, Y.-Z. Song, T. Xiang, T. M. Hospedales, Generalizable person re-identification by domain-invariant mapping network, in: CVPR, 2019, pp. 719–728.

[15] S. Lin, C.-T. Li, A. C. Kot, Multi-domain adversarial feature generalization for person re-identification, IEEE TIP 30 (2020) 1596–1607.

[16] S. Liao, L. Shao, Interpretable and generalizable person re-identification with query-adaptive convolution and temporal lifting, in: ECCV, 2020, pp. 456–474.

[17] S. Choi, T. Kim, M. Jeong, H. Park, C. Kim, Meta batch-instance normalization for generalizable person re-identification, in: CVPR, 2021, pp. 3425–3435.

[18] Y. Dai, X. Li, J. Liu, Z. Tong, L.-Y. Duan, Generalizable person re-identification with relevance-aware mixture of experts, in: CVPR, 2021, pp. 16145–16154.

[19] Z. Li, Y. Sun, L. Zhang, J. Tang, Ctnet: Context-based tandem network for semantic segmentation, IEEE TPAMI.

[20] Z. Li, J. Tang, T. Mei, Deep collaborative embedding for social image understanding, IEEE TPAMI 41 (9) (2018) 2070–2083.

[21] Z. Li, J. Tang, L. Zhang, J. Yang, Weakly-supervised semantic guided hashing for social image retrieval., IJCV 128.

[22] R. A. Güler, N. Neverova, I. Kokkinos, Densepose: Dense human pose estimation in the wild, in: CVPR, 2018, p. 7297–7306.

[23] X. Yang, M. Wang, D. Tao, Person re-identification with metric learning using privileged information, IEEE TIP 27 (2) (2017) 791–805.

[24] X. Yang, M. Wang, R. Hong, Q. Tian, Y. Rui, Enhancing person re-identification in a self-trained subspace, ACM TOMM 13 (3) (2017) 1–23.

[25] M. Wang, H. Li, D. Tao, K. Lu, X. Wu, Multimodal graph-based reranking for web image search, IEEE TIP 21 (11) (2012) 4649–4661.

[26] X. Yang, X. Du, M. Wang, Learning to match on graph for fashion compatibility modeling, in: AAAI, 2020, pp. 287–294.

[27] M. Wang, R. Hong, G. Li, Z.-J. Zha, S. Yan, T.-S. Chua, Event driven web video summarization by tag localization and key-shot identification, IEEE TMM 14 (4) (2012) 975–985.

[28] M. Wang, X. Liu, X. Wu, Visual classification by l1-hypergraph modeling, IEEE TKDE 27 (9) (2015) 2564–2574.

[29] X. Xu, L. Liu, X. Zhang, W. Guan, R. Hu, Rethinking data collection for person re-identification: active redundancy reduction, PR 113 (2021) 107827.

[30] Y. Huang, Z.-J. Zha, X. Fu, W. Zhang, Illumination-invariant person re-identification, in: ACM MM, 2019, p. 365–373.

[31] Z. Zeng, Z. Wang, Z. Wang, Y. Zheng, Y.-Y. Chuang, S. Satoh, Illumination-adaptive person re-identification, IEEE TMM 22 (12) (2020) 3064–3074.

[32] Y.-C. Chen, Y.-J. Li, X. Du, Y.-C. F. Wang, Learning resolution-invariant deep representations for person re-identification, in: AAAI, 2019, pp. 8215–8222.

[33] J. Jiao, W.-S. Zheng, A. Wu, X. Zhu, S. Gong, Deep low-resolution person re-identification, in: AAAI, 2018, pp. 6967–6974.

[34] Y.-J. Li, Y.-C. Chen, Y.-Y. Lin, X. Du, Y.-C. F. Wang, Recover and identify: A generative dual model for cross-resolution person re-identification, in: ICCV, 2019, pp. 8089–8098.

[35] Z. Cheng, Q. Dong, S. Gong, X. Zhu, Inter-task association critic for cross-resolution person re-identification, in: CVPR, 2020, pp. 2605–2615.

[36] R. R. Varior, B. Shuai, J. Lu, D. Xu, G. Wang, A siamese long short-term memory architecture for human re-identification, in: ECCV, 2016, p. 135–153.

[37] W. Li, X. Zhu, S. Gong, Harmonious attention network for person re-identification, in: CVPR, 2018, p. 2285–2294.

[38] X. Bai, M. Yang, T. Huang, Z. Dou, R. Yu, Y. Xu, Deep-person: Learning discriminative deep features for person re-identification, PR 98 (2020) 107036.

[39] Y. Sun, L. Zheng, Y. Yang, Q. Tian, S. Wang, Beyond part models: Person retrieval with refined part pooling (and a strong convolutional baseline), in: ECCV, 2018, pp. 501–518.

[40] G. Wang, Y. Yuan, X. Chen, J. Li, X. Zhou, Learning discriminative features with multiple granularities for person re-identification, in: ACM MM, 2018, p. 274–282.

[41] D. Cheng, Y. Gong, S. Zhou, J. Wang, N. Zheng, Person re-identification by multi-channel parts-based cnn with improved triplet loss function, in: CVPR, 2016, pp. 1335–1344.

[42] W. Li, R. Zhao, T. Xiao, X. Wang, Deepreid: Deep filter pairing neural network for person re-identification, in: CVPR, 2014, pp. 152–159.

[43] H. Luo, W. Jiang, X. Zhang, X. Fan, J. Qian, C. Zhang, Alignedreid++: Dynamically matching local information for person re-identification, PR 94 (2019) 53–61.

[44] W. Li, X. Zhu, S. Gong, Person re-identification by deep joint learning of multi-loss classification, in: IJCAI, 2017, pp. 2194–2200.

[45] Y. Ge, Z. Li, H. Zhao, G. Yin, S. Yi, X. Wang, H. Li, Fd-gan: Pose-guided feature distilling gan for robust person re-identification, in: NeurIPS, 2017, pp. 4627–4635.

[46] Y. Sun, Q. Xu, Y. Li, C. Zhang, Y. Li, S. Wang, J. Sun, Perceive where to focus: Learning visibility-aware part-level features for partial person re-identification, in: CVPR, 2019, pp. 393–402.

[47] H. Yao, S. Zhang, R. Hong, Y. Zhang, C. Xu, Q. Tian, Deep representation learning with part loss for person re-identification, IEEE TIP 28 (6) (2019) 2860–2871.

[48] D. Li, X. Chen, Z. Zhang, K. Huang, Learning deep context-aware features over body and latent parts for person re-identification, in: CVPR, 2017, pp. 384–393.

[49] H. Zhao, M. Tian, S. Sun, J. Shao, J. Yan, S. Yi, X. Wang, X. Tang, Spindle net: Person re-identification with human body region guided feature decomposition and fusion, in: CVPR, 2017, pp. 907–915.

[50] L. Zheng, Y. Huang, H. Lu, Y. Yang, Pose-invariant embedding for deep person re-identification, IEEE TIP 28 (9) (2019) 4500–4509.

[51] L. Wei, S. Zhang, H. Yao, W. Gao, Q. Tian, Glad: Global-local-alignment descriptor for pedestrian retrieval, in: ACM MM, 2017, p. 420–428.

[52] C. Su, J. Li, S. Zhang, J. Xing, W. Gao, Q. Tian, Pose-driven deep convolutional model for person re-identification, in: ICCV, 2017, pp. 3960–3969.

[53] Y. Suh, J. Wang, S. Tang, T. Mei, K. M. Lee, Part-aligned bilinear representations for person re-identification, in: ECCV, 2018, pp. 418–437.

[54] M. S. Sarfraz, A. Schumann, A. Eberle, R. Stiefelhagen, A pose-sensitive embedding for person re-identification with expanded cross neighborhood re-ranking, in: CVPR, 2018, pp. 420–429.

[55] Z. Zhang, C. Lan, W. Zeng, Z. Chen, Densely semantically aligned person re-identification, in: CVPR, 2019, pp. 667–676.

[56] K. He, X. Zhang, S. Ren, J. Sun, Deep residual learning for image recognition, in: CVPR, 2016, pp. 770–778.

[57] W. Li, X. Wang, Locally aligned feature transforms across views, in: CVPR, 2013, pp. 3594–3601.

[58] Z. Zhong, L. Zheng, D. Cao, S. Li, Re-ranking person re-identification with k-reciprocal encoding, in: CVPR, 2017, pp. 1318–1327.

[59] T. Xiao, S. Li, B. Wang, L. Lin, X. Wang, Joint detection and identification feature learning for person search, in: CVPR, 2017, pp. 3415–3424.

[60] L. Zheng, L. Shen, L. Tian, S. Wang, J. Wang, Q. Tian, Scalable person re-identification: A benchmark, in: ICCV, 2015, pp. 1116–1124.

[61] Z. Zheng, L. Zheng, Y. Yang, Unlabeled samples generated by gan improve the person re-identification baseline in vitro, in: ICCV, 2017, pp. 3774–3782.

[62] D. Gray, H. Tao, Viewpoint invariant pedestrian recognition with an ensemble of localized features, in: ECCV, 2008, pp. 262–275.

[63] M. Hirzer, C. Beleznai, P. M. Roth, H. Bischof, Person re-identification by descriptive and discriminative classification, in: SCIA, 2011, pp. 91–102.

[64] C. C. Loy, C. Liu, S. Gong, Person re-identification by manifold ranking, in: ICIP, 2013, pp. 3567–3571.

[65] W.-S. Zheng, S. Gong, T. Xiang, Associating groups of people., in: BMVC, 2009, pp. 1–11.

[66] J. Deng, W. Dong, R. Socher, L.-J. Li, K. Li, L. Fei-Fei, Imagenet: A large-scale hierarchical image database, in: CVPR, 2009, pp. 248–255.

[67] K. He, X. Zhang, S. Ren, J. Sun, Delving deep into rectifiers: Surpassing human-level performance on imagenet classification, in: ICCV, 2015, pp. 1026–1034.

[68] Y. Wang, L. Wang, Y. You, X. Zou, V. Chen, S. Li, G. Huang, B. Hariharan, K. Q. Weinberger, Resource aware person re-identification across multiple resolutions, in: CVPR, 2018, pp. 8042–8051.

[69] Z. Zhong, L. Zheng, G. Kang, S. Li, Y. Yang, Random erasing data augmentation, in: AAAI, 2020, pp. 13001–13008.

[70] C. Wang, Q. Zhang, C. Huang, W. Liu, X. Wang, Mancs: A multi-task attentional network with curriculum sampling for person re-identification, in: ECCV, 2018, pp. 384–400.

[71] P. Luo, R. Zhang, J. Ren, Z. Peng, J. Li, Switchable normalization for learning-to-normalize deep representation, IEEE TPAMI 43 (2) (2019) 712–728.

[72] X. Qian, Y. Fu, T. Xiang, Y.-G. Jiang, X. Xue, Leader-based multi-scale attention deep architecture for person re-identification, IEEE TPAMI 42 (2) (2019) 371–385.

[73] X. Pan, P. Luo, J. Shi, X. Tang, Two at once: Enhancing learning and generalization capacities via ibn-net, in: ECCV, 2018, pp. 464–479.

[74] K. Zhou, Y. Yang, A. Cavallaro, T. Xiang, Learning generalisable omni-scale representations for person re-identification, IEEE TPAMI (2021) 1–1.

[75] Y. Fu, Y. Wei, Y. Zhou, H. Shi, G. Huang, X. Wang, Z. Yao, T. Huang, Horizontal pyramid matching for person re-identification, in: AAAI, 2019, pp. 8295–8302.

[76] Y. Zhao, X. Yu, Y. Gao, C. Shen, Learning discriminative region representation for person retrieval, PR 121 (2022) 108229.

[77] M. M. Kalayeh, E. Basaran, M. Gökmen, M. E. Kamasak, M. Shah, Human semantic parsing for person re-identification, in: CVPR, 2018, pp. 1062–1071.

[78] J. Liu, B. Ni, Y. Yan, P. Zhou, S. Cheng, J. Hu, Pose transferrable person re-identification, in: CVPR, 2018, pp. 4099–4108.

[79] J. Miao, Y. Wu, Y. Yang, Identifying visible parts via pose estimation for occluded person re-identification, IEEE TNNLS.

[80] X. Jin, C. Lan, W. Zeng, G. Wei, Z. Chen, Semantics-aligned representation learning for person re-identification, in: AAAI, 2020, pp. 11173–11180.